

A ubiquitous waste as a superior adsorbent for methylene blue removal: Cow-hair biochar

Esteban Euti^{1,2}, Luciana Morel^{3,4}, Fernanda Stragliotto², Guillermina Luque^{3,4}, María Victoria Bracamonte^{1,5,*}

¹ Faculty of Chemical Sciences, National University of Córdoba (UNC), Córdoba 5000, Argentina

² Enrique Gaviola Institute of Physics (IFEG), National Council on Scientific and Technical Research (CONICET), Córdoba 5000, Argentina

³ Department of Theoretical and Computational Chemistry, Faculty of Chemical Sciences, National University of Córdoba (UNC), Córdoba 5000, Argentina

⁴ Institute of Physical-Chemistry Research of Córdoba (INFIQC), National Council on Scientific and Technical Research (CONICET), Córdoba 5000, Argentina

⁵ Department of Physical-Chemistry, Faculty of Chemical Sciences, National University of Córdoba (UNC), Córdoba 5000, Argentina

* **Corresponding author:** María Victoria Bracamonte, mvbracamonte@unc.edu.ar

CITATION

Euti E, Morel L, Stragliotto F, et al. A ubiquitous waste as a superior adsorbent for methylene blue removal: Cow-hair biochar. *Materials Technology Reports*. 2025; 3(1): 2109.
<https://doi.org/10.59400/mtr2109>

ARTICLE INFO

Received: 21 November 2024

Accepted: 17 January 2025

Available online: 14 February 2025

COPYRIGHT



Copyright © 2025 by author(s). *Materials Technology Reports* is published by Academic Publishing Pte. Ltd. This work is licensed under the Creative Commons Attribution (CC BY) license.
<https://creativecommons.org/licenses/by/4.0/>

Abstract: The efficient and sustainable removal of organic dyes from wastewater remains a critical environmental challenge. In this study, cow hair, an abundant and underutilized agricultural waste, is transformed into biochar through a simple pyrolysis process to develop an effective and eco-friendly adsorbent for methylene blue (MB) dye removal. The physicochemical properties of the cow-hair biochar, including its surface area, porosity, and functional groups, were systematically analyzed to understand its adsorption performance. Batch adsorption experiments were conducted under varying conditions of pH, initial dye concentration, contact time, and pH to evaluate the adsorption efficiency of cow hair biochar. The results revealed that the biochar exhibits superior adsorption capacity for MB, driven by a combination of electrostatic interactions, π - π stacking, and surface oxygen functional group interactions. Using R^2 as criteria, the best-fitting model was the Temkin isotherm, indicating a monolayer adsorption process with a maximum adsorption capacity surpassing many conventional adsorbents, achieving high levels of MB adsorption capacity of 730 mg/g. This study highlights the potential of converting cow hair waste into a high-performance adsorbent, offering a cost-effective and sustainable solution for dye-contaminated wastewater treatment. The findings pave the way for innovative waste valorization strategies and contribute to the advancement of green environmental technologies.

Keywords: adsorption; cow-hair biochar; methylene blue; wastewater treatment

1. Introduction

Dyes are used in different industries, such as textiles, plastics, paper, rubber, leather, and food, among others, to impart color to different products. The use of these substances presents a series of disadvantages, such as their toxicity and persistence in nature [1]. This is why the indiscriminate disposal of wastewater contaminated with dyes in natural effluents represents a major problem reflected in the impact on both the flora and fauna of the affected ecosystems.

Among the most used dyes, MB is a cationic structure that, although not extremely toxic, can produce Heinz bodies, cyanosis, jaundice, and necrosis [2]. Due to these reasons, it is used as a model molecule for the study of the use of adsorbents for effluent treatment. The global production of MB, estimated at 42,000–49,000 tons annually [3], primarily supports medical, laboratory, and industrial applications, including its use in treating certain poisonings and as a cell-staining agent. While only

a small fraction of the total production is released into the environment, studies suggest that 100–500 tons per year may enter water bodies and soils through industrial effluents. At high concentrations, MB can harm aquatic ecosystems by disrupting photosynthesis and affecting sensitive organisms, though many countries have implemented wastewater treatment regulations to mitigate its environmental impact.

It should be noted that the removal of dyes from wastewater involves a difficult task since there is no unified treatment or procedure [1]. Various treatment processes have been applied for this purpose, such as photocatalytic degradation [4], sonochemical degradation [5], improved micellar ultrafiltration [6], removal by cation exchange membranes [7], electrochemical degradation [8], chemical and biological degradation [9], among others [10]. However, most of these strategies have high costs or can produce subproducts even more toxic than the original one. Despite the numerous physicochemical methods tested, adsorption stands out as the most effective option [11,12]. This is attributed to its simple design, ease of operation, high efficiency, biodegradability, cost-effectiveness, widespread availability, and capacity to handle dyes at higher concentrations [13]. Activated carbons are known for their excellent adsorption capabilities for a wide range of organic substances. Nevertheless, their high cost can limit their application [14]. This has led researchers to explore more cost-effective alternatives, such as carbon, fly ash, silica gel, wool waste, agricultural by-products, wood residues, and clay-based materials. The use of biochar as an adsorbent material has attracted increasing attention due to its high porosity, large surface area, high adsorption capacity, and relatively low cost [15–17]. Biochar can be produced from a wide range of biomass sources, including agricultural waste, such as cow hair [18]. In 2014, the total annual global leather production reaches approximately 24 billion sq. ft tons, 5 billion sq. ft in Europe, and 11.2 billion sq. ft in Asian countries [19,20], with the latter being the largest producer. The industry relies heavily on the meat sector for raw hides and supplies major markets such as fashion, automotive, and footwear. However, it generates significant chemical and organic waste, presenting environmental challenges, especially in regions with less stringent regulations.

In the present work, cow hair biochar from the tannery industry was used for the first time for the adsorption of MB with a high adsorption capacity thanks to its physicochemical properties. The study looks at the effects of contact time, MB concentration, initial pH, adsorbent concentration, adsorption kinetics analysis, equilibrium models, and thermodynamics were also investigated. The adsorption capability was further tested with real water samples.

2. Materials and methods

2.1. Chemicals and reagents

Cow-hair material was collected from Arlei's tannery industry, Corrientes (Argentina). Potassium hydroxide (KOH) and hydrochloric acid (HCl, 36.5%–38%) were from Cicarelli. MB and ethanol were purchased from Sigma Aldrich. All the chemicals were reagent grade and used without further purification. All solutions were prepared with ultra-pure water from a Millipore MillQ system. Real samples from the

Suquía River were taken directly from the river and used with a previous filtering process (paper filter 0.44 μm).

2.2. Biochar preparation

The raw cow hair was dried at 80 °C for 18 h and used without any further purification or washing process. After drying, the cow hair was carbonized at 500 °C for 30 min in the N_2 atmosphere. The obtained biochar was mixed with KOH solution with a concentration of 8 wt% to get a 1:1 ratio of biochar: KOH. The mixture was magnetically stirred for 2 h and then heated to 80 °C until the solvent was fully evaporated. The obtained powder was thermally treated at 900 °C for 1 h under N_2 atmosphere. In every case, a heating ramp of 5 °C/min was used. After the sample cooled down, it was washed thoroughly with HCl with a concentration of 7 wt% and water until neutral pH was reached (**Figure 1**). As a reference, the same thermal process was applied to another sample without the chemical activation. The samples are named CHB-NA (non-activated cow-hair biochar) and CHB-A (activated cow-hair biochar). KOH activation is well known to easily allow the formation of micropores, resulting in high-surface-area biocarbons, which favors the adsorption of contaminants [18,21,22].

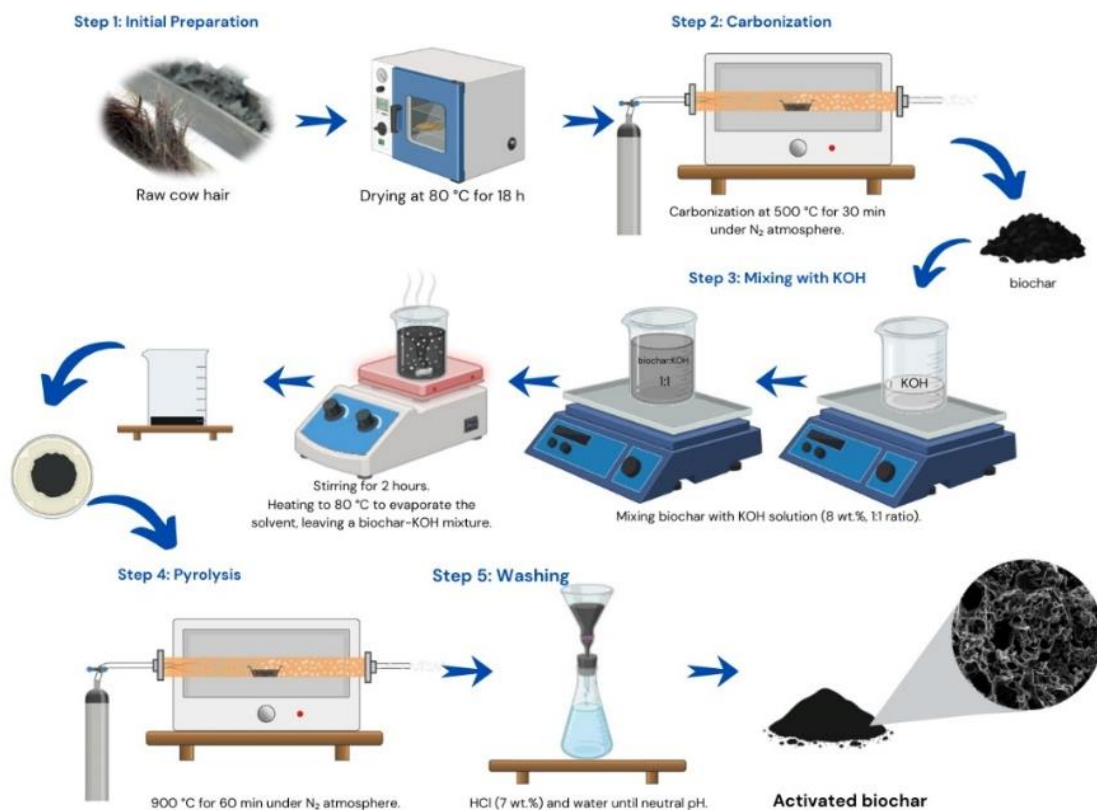


Figure 1. Synthesis procedure of CHB-A biocarbon.

2.3. Materials characterization

The synthesized biocarbons were characterized by X-ray diffractometry (XRD) collected on a Pan-Analytical diffractometer with the $\text{Cu-K}\alpha$ radiation ($\lambda = 1.5406 \text{ \AA}$). The different biocarbon morphologies were characterized by Scanning Electron Microscopy (SEM) with a field emission scanning electron microscope (FE-SEM),

Sigma Zeiss (LAMARX facilities). Elemental analysis was performed on an energy-dispersive X-ray (EDS) spectrometer attached to an FE-SEM. Thermogravimetric analysis was performed on a thermogravimetric analyzer (TGA, Q500, TA Instrument Corporation) in a nitrogen atmosphere with a heating rate of 10 °C/min from room temperature to 700 °C. Brunauer-Emmett-Teller (BET) surface area and total micro- and mesopore volume of the biochars were measured at least in duplicate by nitrogen gas sorption at 77 K using a NOVA 1000e porosimeter (Quantachrome, Boynton Beach, FL, USA). The total pore volume was calculated using Gurvich's rule at $p/p^0 = 0.98$ [23], while the micropore area and volume were determined using the α -plot method with the NPC standard isotherm [24]. UV-Vis determinations were performed in a UV/Vis spectrophotometer Jenway (model 6705) using quartz cells.

2.4. Adsorption experiments

MB was used as an adsorbate for batch adsorption experiments. The adsorption isotherm experiments were performed using an aqueous solution with MB concentration variable at room temperature (25 °C). The MB concentration was analyzed by UV spectroscopy.

The adsorbed amount and removal efficiency (η) were calculated according to:

$$q_e = \frac{(C_0 - C_e)}{m} V \quad (1)$$

$$\eta = \frac{C_0 - C_e}{C_0} \times 100\% \quad (2)$$

where q_e is the adsorption capacity (mg/g), C_0 and C_e are the initial and equalized concentrations of MB (mg/L), m is the adsorbent mass (g), V is the volume (L) of MB solution, and η is the removal efficiency [25].

The adsorption thermodynamics was analyzed using three different isotherm models: Langmuir (Equation (3)), Freundlich (Equation (4)), and Temkin (Equation (5)).

$$\frac{C_e}{q_e} = \frac{1}{(q_m K_L)} + \frac{C_e}{q_m} \quad (3)$$

$$\ln q_e = \ln(K_F) + \frac{1}{n} \ln(C_e) \quad (4)$$

$$q_e = \left(\frac{RT}{b_T}\right) \ln A_T + \left(\frac{RT}{b_T}\right) \ln(C_e) \quad (5)$$

where q_e (mg/g) is the equilibrium adsorption capacity, C_e (mg/L) is the equilibrium concentration of MB solution, q_m (mg/g) is the maximum adsorption capacity of adsorbent, K_L (L/mg) is the Langmuir constant, K_F (mg/g) is an indicator of adsorption capacity and n is an indicator of intensity, R is the gas constant, T the temperature, b_T is the Temkin constant and A_T is the Temkin isotherm constant [25].

Pseudo-first and pseudo-second-order kinetic models (Equations (6) and (7)) were used to analyze the data:

$$q_t = q_e(1 - e^{-k_1 t}) \quad (6)$$

$$\frac{t}{q_t} = \frac{1}{(k_2 q_e^2)} + \frac{t}{q_e} \quad (7)$$

where q_e and q_t are the amount of adsorbed MB and the equilibrium and t time, respectively. k_1 and k_2 (mg/g·h) are the first and second-order rate constants, respectively. Adsorption experiments obtained from diverse biochar batches and screened under identical conditions were found to display a performance variability of < 10% in terms of absorbance.

3. Results and discussion

3.1. Material characterization

The microscopic structure and the composition of CHB-NA and CHB-A were evaluated by SEM and XRD measurements, respectively. **Figures 2A,B** show the SEM images of CHB-NA and CHB-A samples, respectively.

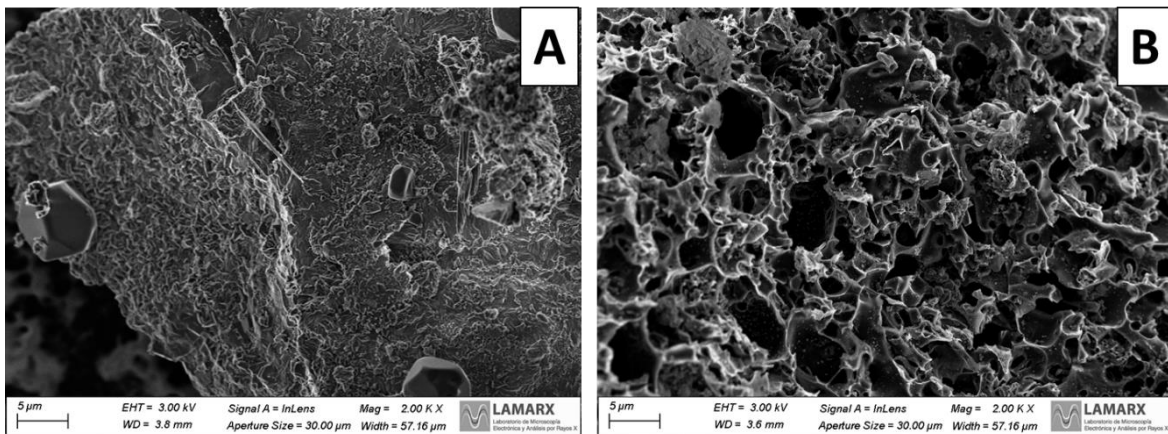


Figure 2. SEM images of CHB-NA (A) and CHB-A (B) samples.

As can be seen in **Figure 2B**, the activated sample presents a more open structure with respect to the non-activated one. The morphology of CHB-A seems as if wrinkled nanosheets are connected, forming a structure with open pores indicating a higher surface area due to the activation process. A further analysis was performed by XRD, **Figure 3**. For the non-activated sample (**Figure 3A**), the two typical amorphous carbon peaks at 26.5° and 44° are not visible, while other signals coming from impurities present in the raw material are evidenced. In the case of the activated sample (**Figure 3B**), the peaks corresponding to the (002) and (101) planes are present, indicating graphene-like carbon materials [26]. These results indicate that the activation process not only promotes the graphitization but also reduces the amount of impurities in the final sample [18].

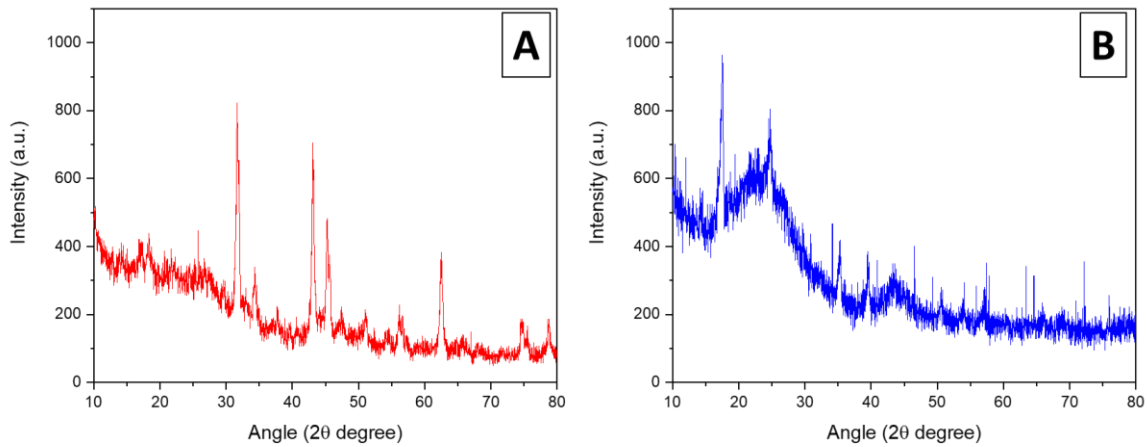


Figure 3. X-Ray diffractograms for CHB-NA (A) and CHB-A (B).

The surface area and pore volume of both biochars were examined by N_2 adsorption/desorption isotherms (Figure 4), and the results are summarized in Table 1.

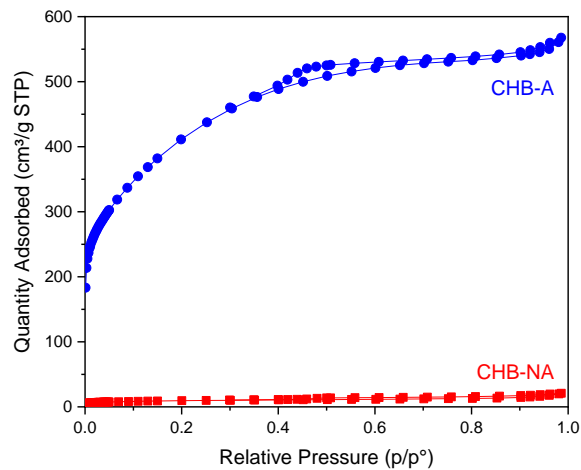


Figure 4. N_2 adsorption-desorption isotherm for CHB-NA (red squares) and CHB-A (blue circles).

Table 1. Morphology parameters obtained from N_2 -sorption analysis.

Sample	S_{BET} (m^2/g)	S_{Meso} (m^2/g)	S_{Micro} (m^2/g)	V_{PT} (cm^3/g)	V_{Meso} (cm^3/g)	V_{Micro} (cm^3/g)
CHB-NA	34	20	14	0.03	0.024	0.006
CHB-A	1468	1191	277	0.88	0.77	0.11

According to the IUPAC classification, CHB-NA and CHB-A present a type IV isotherm [27], indicating the presence of micro- and mesopores in the structure. However, the specific surface area of CHB-A ($1468 m^2/g$) is 44 times higher than that of CHB-NA, which is consistent with the higher porosity previously observed by SEM. Moreover, the higher V_{Meso} and V_{Micro} obtained for the activated sample highlight the importance of the KOH activation [7,18,28] since the higher surface area can

promote higher adsorption of MB, while the presence of meso and micropores allows the diffusion of MB to the internal part of the carbonaceous structure, playing a crucial role in the adsorption capacity of CHB-A [29–31].

3.2. Adsorption experiments

3.2.1. Effect of contact time

The sorption ability of the activated and non-activated biochars (0.2 g/L) towards a 10 mg/L MB solution was studied over a contact time of up to 5 min at ambient conditions. The dye uptake was evaluated by UV-Vis spectroscopy, fixing the wavelength in 665.5 nm according to the calibration curve performed (Figure S1, supporting information). The maximum contact time was determined based on the point at which no significant changes in absorbance were observed. This ensured that the system had reached equilibrium, allowing for reliable analysis of the adsorption process.

The analysis of absorbance as a function of time for CHB-NA and CHB-A is presented in Figure 5. The measurement using commercial activated carbon (AC) is included as a reference for the analysis.

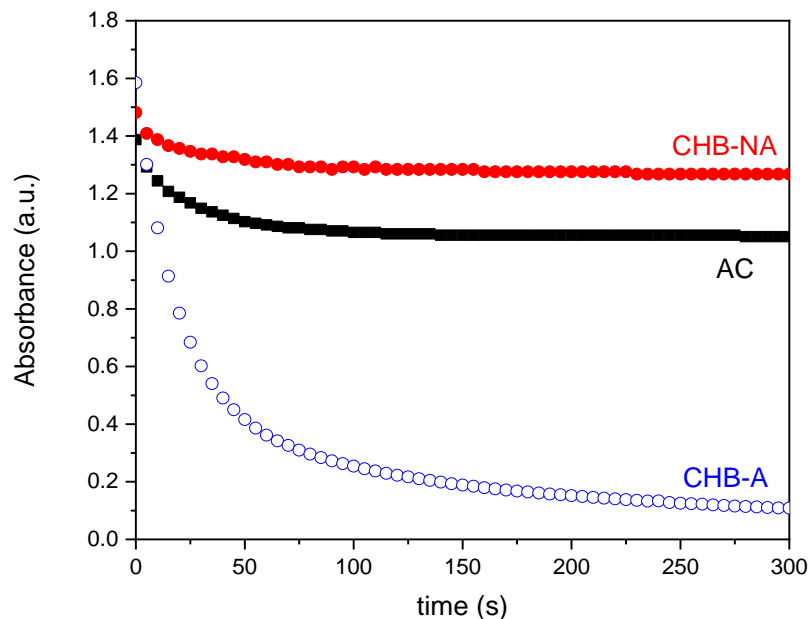


Figure 5. Absorbance vs. time changes during MB uptake on activated carbon (black squares), CHB-NA (full red circles) and CHB-A (empty blue circles).

As can be seen, after the addition of each carbon material, the absorbance rapidly decreases, reaching values of 1.1, 1.3 and 0.1 for AC, CHB-NA and CHB-A, respectively. The equilibrium condition was reached after 5 min for every sample. Table 2 presents the calculated removal efficiency and adsorption capacity for AC, CHB-NA and CHB-A. As can be seen, the highest removal efficiency was obtained for CHB-A. The higher the content of oxygenated groups should be associated with the highest the removal capacity of the dye as was recently reported by Charmas et al. [32].

Table 2. Removal efficiency and adsorption capacity calculated for each sample.

	AC	CHB-NA	CHB-A
removal efficiency (η)	26.3	15.5	95.6
adsorption capacity (q_e)	6.2	3.6	30.5

3.2.2. Effect of initial MB concentration

The influence of different initial MB concentrations using a 0.85 g/L dosage of CHB-A (the best adsorbent) is shown in **Figure 6**. As observed, the maximum MB uptake for the CHB-A increased from 30 to 570 mg/g. At higher concentrations, the increased mass transfer driving force enables a greater number of MB molecules to migrate toward the adsorbent surfaces. This facilitates the occupation of binding sites, thereby enhancing the adsorption of MB. Note that the MB concentration range was chosen to ensure comparability and consistency with earlier studies in the field.

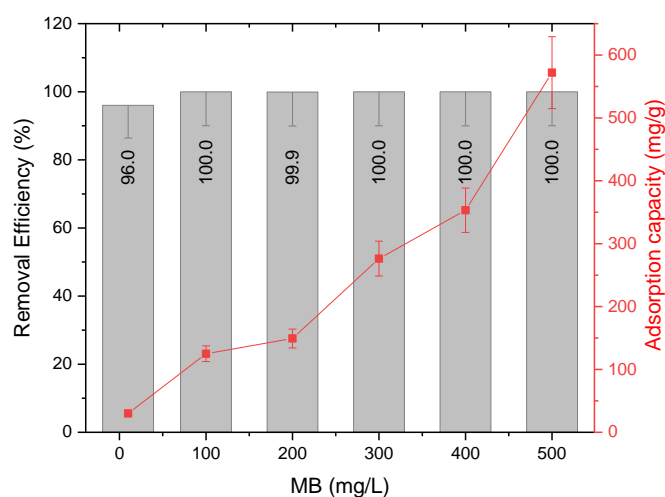


Figure 6. Removal efficiency (grey bars) and adsorption capacity (red squares) on CHB-A in function of the initial dye concentration.

3.2.3. Effect of CHB-A dosage

The effect of the adsorbate-to-adsorbent ratio was evaluated, as it is a key parameter in optimizing an effective and economical dye remover for wastewater treatment. The influence of adsorbent dosage on adsorption was studied by using different amounts of CHB-A while maintaining a fixed MB concentration of 500 mg/L. This approach allowed for the assessment of adsorption efficiency under varying adsorbent quantities, providing insights into the optimal conditions for maximum dye removal. The results are presented in **Figure 7**.

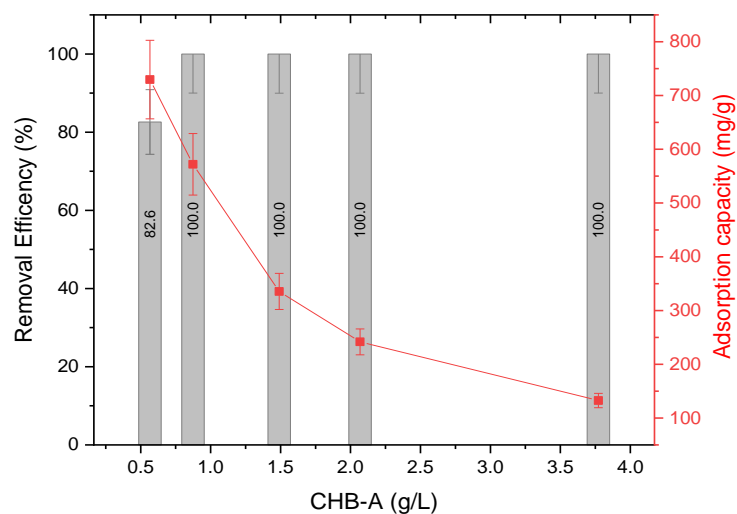


Figure 7. Removal efficiency of the CHB-A material with respect to the adsorbent dose.

The results indicate that even at the lowest concentration of CHB-A, the removal efficiency is maximum (82%) and increases rapidly to 100%. On the other hand, they vary from 730 to 133 when the amount of adsorbent increases. Analyzing Equation (1) used to calculate it, it is possible to note that increasing the amount of CHB-A is possible to enhance the dye uptake.

3.2.4. Effect of pH on the MB adsorption

The impact of the initial pH of a 500 mg/L MB solution was evaluated using 0.8 g/L of CHB-A, and the results are presented in **Figure 8**. The minimum and maximum removal efficiencies were observed at pH 2 and pH 10, respectively. The lower adsorption efficiency at acidic pH levels may be attributed to competition between H^+ ions and dye molecules for the active sites on the biochar surface. Between pH 4 and 10, only a slight increase in removal efficiency was noted, suggesting that MB adsorption is relatively insensitive to initial pH variations. However, at pH values below the isoelectric point of MB (7.2) [33], the solution likely maintains an overall positive charge, leading to electrostatic repulsion and reduced MB uptake.

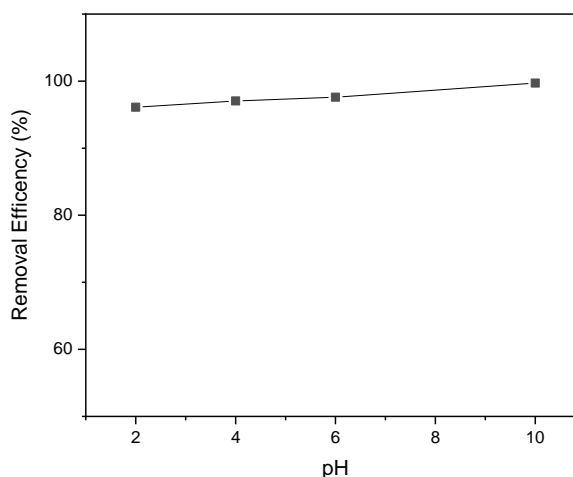


Figure 8. Effect of initial pH of MB solution on dye removal efficiency of CHB-A.

To further investigate the possible mechanism of MB adsorption, the final pH of the solutions was also measured (**Table S1**). In all cases, an increase in pH was observed. This change was more pronounced at lower initial pH values ($\Delta\text{pH} = 3$ at $\text{pH} = 2$) compared to higher initial pH values ($\Delta\text{pH} = 0.2$ at $\text{pH} = 10$). This phenomenon can be attributed to the higher proton consumption associated with the functional groups present on the biochar. At lower pH levels, the presence of positive charges does not favor the adsorption of the dye onto CHB-A. Nevertheless, despite the electrostatic repulsion and/or competition between H^+ ions and MB molecules for adsorption sites, a removal efficiency of 96% was achieved at $\text{pH} = 2$. This indicates the involvement of additional mechanisms in the MB adsorption process. Similar findings have been reported [34,35], suggesting that MB adsorption can alter the isoelectric point of adsorbents.

3.2.5. Adsorption kinetics analysis

Pseudo-first-order and pseudo-second-order kinetic models were tested to fit the data presented in the 3.2.1 section. According to the obtained results, the pseudo-second-order kinetic model is the best for the analysis of the adsorption mechanism. The representative plots and the model parameters are shown in **Figure 9**, **Figure S2**, and **Table 3**, respectively. For a better comparison, commercial activated carbon is also included in the table.

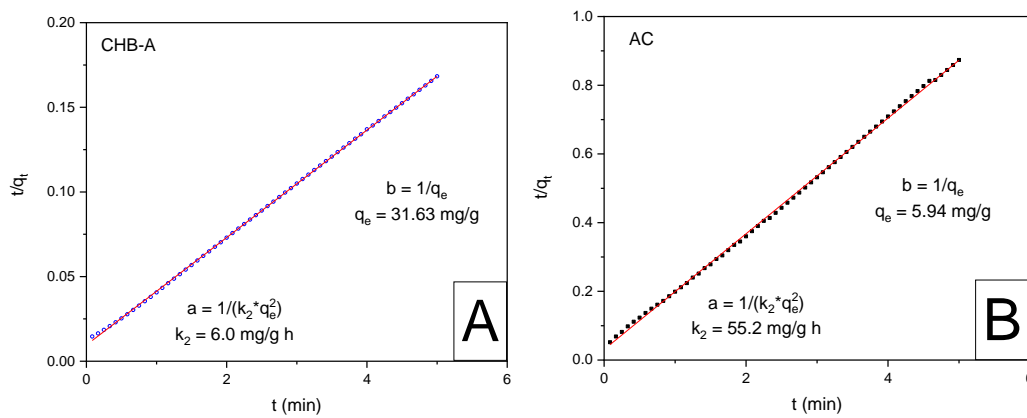


Figure 9. MB adsorption kinetic onto CHB-A (**A**) and AC (**B**) fitted into the pseudo-second-order model.

Table 3. Kinetic parameters for MB adsorption onto CHB-A and AC.

Sample	q_e (mg/g)	k_2 (mg/g·h)	R^2
CHB-A	31.63	6.0	0.99997
AC	5.94	55.2	0.9992

The pseudo-second-order kinetic model predicted a $q_e = 31.63$ mg/g and $k_2 = 6.0$ mg/g·h for CHB-A with a correlation of 0.99997 and $q_e = 5.94$ mg/g and $k_2 = 55.2$ mg/g·h with $R^2 = 0.9992$ for AC. The high R^2 and the coherence between the calculated q_e and the experimental one indicates the suitability of pseudo-second-order kinetic model for the adsorption of MB on each material. k_2 plays an important role as a time of scaling factor, that is, when its value is relatively high, the time required for the

system to reach an equilibrium state is relatively short, a contrary situation occurs for small constants [36,37]. In our case, the smaller k_2 value obtained for the CHB-A material, could be related with several rate limiting aspects that affect the adsorption mechanism. To know the detailed aspects of the adsorption process of MB on CHB-A, the interparticle diffusion (IPD) model was used:

$$q_t = k_p t^{0.5} + C \quad (8)$$

where q_t (mg/g) is the adsorption amount at t ; k_p is the rate constant of the diffusion model in particles, and C is the constant associated with the boundary layer effect [38]. The results are presented in **Figure 10**.

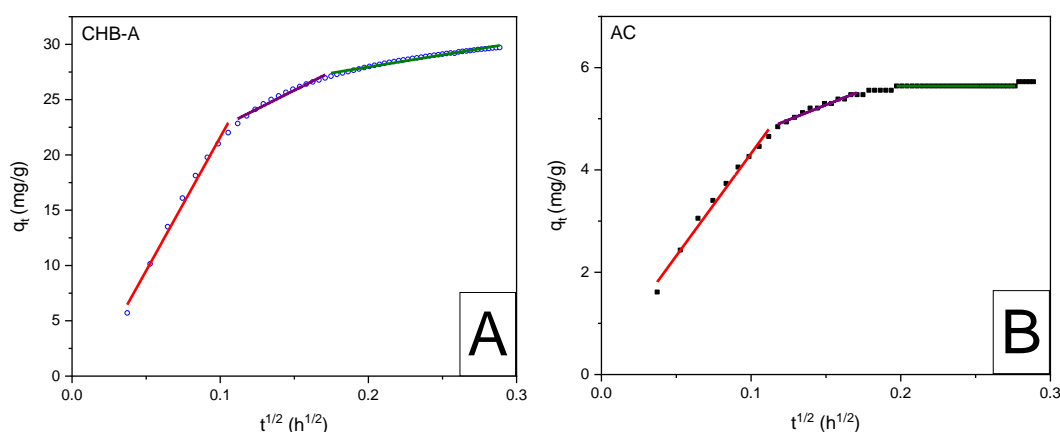


Figure 10. Intra-particle diffusion model for MB adsorption on CHB-A (A) and AC (B).

Both carbons present a three-region plot, which is associated with a first rapid adsorption towards active sites on the surface of the absorbent, a second gradual diffusion of MB molecules towards the pores of the absorbent material and a third stage that corresponds to the diffusion from macro to micro pores [39]. As can be seen from **Table S2**, the values of the rate constant for the particle diffusion model are lower for all AC settings, indicating an increase in diffusion resistance at all stages with respect to CHB-A settings. This is consistent with the studies on surface area and pore volume performed.

3.2.6. Adsorption equilibrium isotherms analysis

The isotherm's plot of the three isotherms analyzed (Langmuir, Freundlich, and Temkin) is presented in **Figure S3**. The parameters extracted from the model are shown in **Table 4**. Using R^2 as criteria, the best-fitting model is Temkin, indicating that the adsorption is characterized by a uniform distribution of binding energies, up to a maximum binding energy.

Table 4. Isotherm parameters for MB adsorption onto CHB-A.

Langmuir		Freundlich		Temkin	
q_m	85.91	n	0.52	b_T	10
K_L	0.54	K_F	135	A_T	2.19
R^2	0.44	R^2	0.60	R^2	0.85

Even though the Temkin model could not perfectly describe the adsorption characteristics, the parameter b_T , related to the adsorption strength, can still serve as a reference to understand the adsorption process. In ion-exchange mechanisms, the typical binding energy ranges from 8 to 16 kJ/mol during chemisorption processes, whereas in physisorption, the value is generally below -40 kJ/mol. These energy values provide valuable insights into the nature of the adsorption mechanism, distinguishing between physical and chemical interactions. In this study, the b_T value of 0.001 kJ/mol indicates that the adsorption process of MB onto CHB-A implies both chemi- and physisorption [40].

A comparative analysis was conducted to evaluate the adsorption capacity of various bio-adsorbents and CHB-A for the removal of MB dye **Table 5**.

Table 5. Comparison of adsorption capacity of CHB-A with other systems.

Adsorbent	q_m (mg/g)	MB concentration	Ref
Magnolia Grandiflora Linn leaf biochar	78.6	200 mg/L	[41]
Ball milled bagasse biochar	354	50 mg/L	[42]
Sheep manure biochar	238.31	50 mg/L	[43]
Modified rice straw biochar	50.27	100 mg/L	[44]
Bamboo biochar	48.14	150 mg/L	[45]
CHB-A	570	500 mg/L	This work

Among the compared biochar, CHB-A demonstrated the highest MB adsorption capacity, far outperforming all other adsorbents listed. Although Magnolia Grandiflora Linn leaf biochar exhibited higher adsorption capacity compared to bamboo and modified rice straw biochar, it was significantly outperformed by ball-milled bagasse biochar and sheep dung biochar. However, the adsorption capacity of CHB-A was notably higher, even at a higher concentration of MB. The exceptional performance of CHB-A can be attributed to its higher specific surface area, abundance of active sites, and the presence of more functional groups, which together enhance its adsorption capabilities.

3.2.7. Adsorbent regeneration and reusability

The real application of an adsorbent is dependent on the possibility of regenerating and reusing it. For this, the reusable performance of CHB-A was evaluated. The regeneration was done according to Martis et al. [46]. Briefly after the MB adsorption, the sample was sonicated with ethanol solvent and washed by centrifugation 5 times. After that, the CHB-A was dried at 80 °C until constant mass, and a new adsorption test was performed using MB 500 mg/L. The results are presented in **Figure 11** and show that even after six cycles, the CHB-A adsorbent retained 86.8% of its MB removal efficiency. This reduction in performance may be associated with the gradual depletion of active adsorption sites on the surface of the composite or potential surface damage over time [47–49].

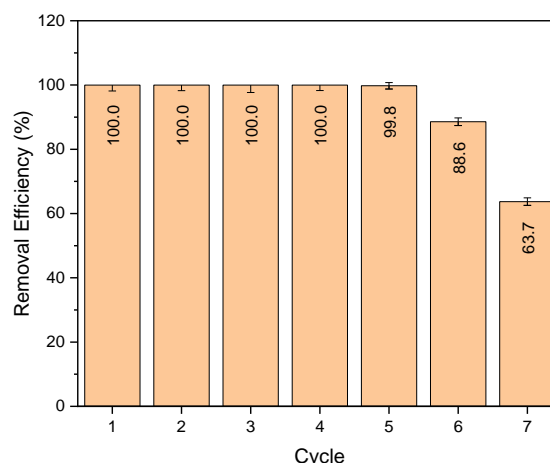


Figure 11. Removal efficiency in function of the number of regeneration cycles.

3.2.8. Proposed mechanism of MB adsorption

According to the results presented above, it can be stated that the adsorption process of MB on biochar is a complicated process. It may involve: external liquid film diffusion, surface adsorption, and intraparticle diffusion. Based in the experimental-DFT study presented by Yu et al. [50] in 2024, the interaction between the biochar and the MB molecule is principally due to H-bonding, π - π and electrostatic interactions between the CHB-A and MB. Pore filling could also be predicted by the intraparticle diffusion model, where three regions were observed indicating that the intraparticle diffusion could also be controlled by, for example, liquid film diffusion and/or adsorption reaction [43] (**Figure 12**).

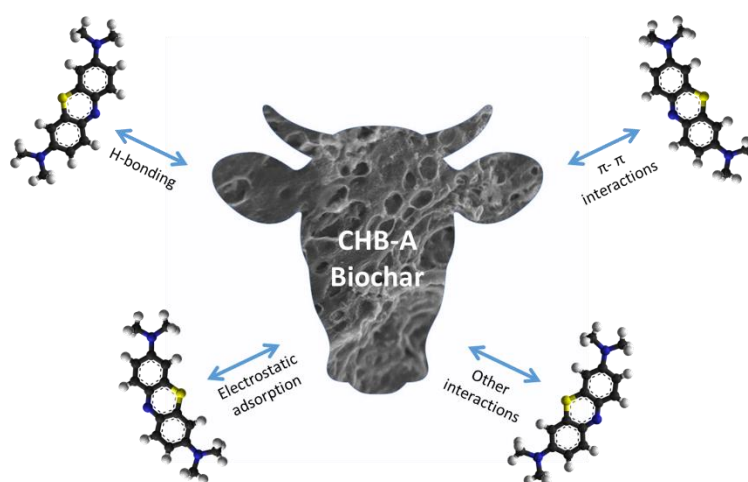


Figure 12. Diagram of the complex adsorption mechanism of MB onto CHB-A.

3.2.9. MB adsorption using contaminated water

The MB adsorption of CHB-A was further tested with real water samples from the Suquía River contaminated with MB to know the practical utility. The CHB-A biochar reduced the MB dye concentration from 500 mg/L to 1.03 mg/L using only 0.005 g of adsorbent for 5 min at room temperature. Compared to the solutions prepared with ultrapure water, the removal efficiency was 99.8%, and the adsorption

capacity was 508 mg/g. The smaller value could be attributed to the presence of other interfering polluting compounds.

4. Conclusions

This study demonstrates the exceptional potential of cow-hair-derived biochar as a highly effective adsorbent for the removal of MB from aqueous solutions. The activated biochar exhibited a high specific surface area of 1468 m²/g and remarkable porosity, attributed largely to KOH activation, which played a critical role in enhancing porosity and sample purity. Adsorption experiments confirmed that CHB-A outperformed commercial activated carbon, achieving an equilibrium adsorption capacity of 730 mg/g. This superior performance is credited to its high porosity and the presence of oxygen functional groups. The adsorption process was well-characterized by the Temkin isotherm model, indicating a uniform distribution of binding energies, while the pseudo-second-order kinetic model provided the best fit for understanding the adsorption mechanism. The pH analysis reveals a complex mechanism for MB adsorption on CHB-A, which may include a combination of hydrogen bonding, electrostatic and Van der Waals interaction, among others. Notably, CHB-A retained its high removal efficiency even after six regeneration cycles, surpassing most biochars reported in the literature for MB adsorption. Additionally, its performance was validated using contaminated water from the Suquía River, highlighting its practical applicability. Given the abundance of cow hair as an agricultural byproduct and the impressive results achieved, this biochar represents a cost-effective, sustainable, and environmentally friendly solution to the challenge of dye-contaminated water treatment.

Supplementary materials: UV-spectrum and the corresponding calibration curve of MB, Fitting of MB adsorption kinetic with the pseudo-second-order model, isotherm analysis and tables with pH analysis and the IPD model's results are presented.

Author contributions: Conceptualization, MVB; methodology, MVB, EE, LM and GL; validation, EE and LM; formal analysis, EE, LM and MVB; investigation, MVB, EE and GL; resources, MVB; data curation, EE, LM, FS and MVB; writing—original draft preparation, EE and MVB; writing—review and editing, MVB and GL; supervision, MVB; project administration, FS; funding acquisition, MVB and GL. All authors have read and agreed to the published version of the manuscript.

Conflict of interest: The authors declare no conflict of interest.

References

1. Al-Tohamy R, Ali SS, Li F, et al. A critical review on the treatment of dye-containing wastewater: Ecotoxicological and health concerns of textile dyes and possible remediation approaches for environmental safety. *Ecotoxicology and Environmental Safety*. 2022; 231: 113160. doi: 10.1016/j.ecoenv.2021.113160.
2. Oladoye PO, Ajiboye TO, Omotola EO, et al. Methylene blue dye: Toxicity and potential elimination technology from wastewater. *Results in Engineering*. 2022; 16: 100678. doi: 10.1016/j.rineng.2022.100678.
3. Djama C, Bouguettoucha A, Chebli D, et al. Experimental and Theoretical Study of Methylene Blue Adsorption on a New Raw Material, *Cynara scolymus*—A Statistical Physics Assessment. *Sustainability*. 2023; 15(13): 10364. doi: 10.3390/su151310364.

4. Mishra S, Sundaram B. A review of the photocatalysis process used for wastewater treatment. *Materials Today: Proceedings*. 2023. doi: 10.1016/j.matpr.2023.07.147.
5. Pirsahab M, Moradi N, Hossini H. Sonochemical processes for antibiotics removal from water and wastewater: A systematic review. *Chemical Engineering Research and Design*. 2023; 189: 401–439.
6. Aryanti N, Nafiunisa A, Giraldi VF, et al. Separation of organic compounds and metal ions by micellar-enhanced ultrafiltration using plant-based natural surfactant (saponin). *Case Studies in Chemical and Environmental Engineering*. 2023; 8: 100367. doi: 10.1016/j.cscee.2023.100367.
7. Chauhan MS, Rahul AK, Shekhar S, et al. Removal of heavy metal from wastewater using ion exchange with membrane filtration from Swarnamukhi river in Tirupati. *Materials Today: Proceedings*. 2023; 78: 1–6. doi: 10.1016/j.matpr.2022.08.280.
8. Najafinejad MS, Chianese S, Fenti A, et al. Application of Electrochemical Oxidation for Water and Wastewater Treatment: An Overview. *Molecules*. 2023; 28(10): 4208. doi: 10.3390/molecules28104208.
9. Ma W, Zhang X, Han H, et al. Overview of enhancing biological treatment of coal chemical wastewater: New strategies and future directions. *Journal of Environmental Sciences*. 2024; 135: 506–520. doi: 10.1016/j.jes.2022.11.008.
10. Sarria V, Deront M, Péringer P, et al. Degradation of a biorecalcitrant dye precursor present in industrial wastewaters by a new integrated iron (III) photoassisted–biological treatment. *Applied Catalysis B: Environmental*. 2003; 40(3): 231–246. doi: 10.1016/S0926-3373(02)00162-5.
11. Bulut Y, Aydın H. A kinetics and thermodynamics study of methylene blue adsorption on wheat shells. *Desalination*. 2006; 194(1–3): 259–267. doi: 10.1016/j.desal.2005.10.032.
12. Chen X. Fabrication of Core-Shell Hydrogel Bead Based on Sodium Alginate and Chitosan for Methylene Blue Adsorption. *JRM*. 2024; 12(4): 815–826. doi: 10.32604/jrm.2024.048470.
13. Sanghi R, Bhattacharya B. Review on decolorisation of aqueous dye solutions by low cost adsorbents. *Coloration Technology*. 2006; 118: 256–259.
14. Shukla SK, Al Mushaiqri NRS, Al Subhi HM, et al. Low-cost activated carbon production from organic waste and its utilization for wastewater treatment. *Applied Water Science*. 2020; 10. doi: 10.1007/s13201-020-1145-z.
15. Angin D. Effect of pyrolysis temperature and heating rate on biochar obtained from pyrolysis of safflower seed press cake. *Bioresource Technology*. 2013; 128: 593–597. doi: 10.1016/j.biortech.2012.10.150.
16. Holanda MAS, Coelho Menezes JM, Coutinho HDM, et al. Effectiveness of biochar as an adsorbent for pesticides: Systematic review and meta-analysis. *Journal of Environmental Management*. 2023; 345: 118719. doi: 10.1016/j.jenvman.2023.118719.
17. Ji G, Xing Y, You T. Biochar as adsorbents for environmental microplastics and nanoplastics removal. *Journal of Environmental Chemical Engineering*. 2024; 12(5): 113377. doi: 10.1016/j.jece.2024.113377.
18. Bracamonte MV, Luque GL, Calderón CA, et al. Sustainable Cow Hair Biocarbon-Sulfur Cathodes with Enhanced Electrochemical Performance. *ChemistrySelect*. 2023; 8(42): e202302443. doi: 10.1002/slct.202302443.
19. Dowlath MJH, Karuppannan SK, Rajan P, et al. Chapter Seven-Application of advanced technologies in managing wastes produced by leather industries—An approach toward zero waste technology. In: Hussain CM (editor). *Concepts of Advanced Zero Waste Tools*. Elsevier; 2021. pp. 143–179. doi: 10.1016/B978-0-12-822183-9.00007-6.
20. U.S. Leather and Hide Industry 2020 Year End Review; 2021 Projections | LHCA, (n.d.). https://www.usleather.org/press/US_Hide_Skin_Leather_Industry_2020_Year_End_Data_2021_Projections (accessed 16 December 2024).
21. Raviolo S, Bracamonte MV, Suarez Ramanzin MB, et al. Valorization of brewer’s spent grain via systematic study of KOH activation parameters and its potential application in energy storage. *Biomass and Bioenergy*. 2025; 192: 107494. doi: 10.1016/j.biombioe.2024.107494.
22. Zandifar A, Esmaeilzadeh F, Rodríguez-Mirasol J. Hydrogen-rich gas production via supercritical water gasification (SCWG) of oily sludge over waste tire-derived activated carbon impregnated with Ni: Characterization and optimization of activated carbon production. *Environmental Pollution*. 2024; 342: 123078. doi: 10.1016/j.envpol.2023.123078.
23. Rouquerol F, Rouquerol J, Sing K. *Front Matter*. In: *Adsorption by Powders and Porous Solids*. Academic Press; 1999. p. iii. doi: 10.1016/B978-0-12-598920-6.50017-8.

24. Desmurs L, Galarneau A, Cammarano C, et al. Determination of Microporous and Mesoporous Surface Areas and Volumes of Mesoporous Zeolites by Corrected t-Plot Analysis. *ChemNanoMat*. 2022; 8(4): e202200051. doi: 10.1002/cnma.202200051.
25. Xue H, Wang X, Xu Q, et al. Adsorption of methylene blue from aqueous solution on activated carbons and composite prepared from an agricultural waste biomass: A comparative study by experimental and advanced modeling analysis. *Chemical Engineering Journal*. 2022; 430: 132801. doi: 10.1016/j.cej.2021.132801.
26. Raviolo S, Bracamonte MV, Calderón CA, et al. A Green Solution to Energy Storage: Brewers' Spent Grains Biocarbon–Silica Composites as High-Performance Lithium-Ion Batteries Anodes. *Energy Technology*. 2023; 11(9): 2300342. doi: 10.1002/ente.202300342.
27. Donohue MD, Aranovich GL. Classification of Gibbs adsorption isotherms. *Advances in Colloid and Interface Science*. 1998; 76–77: 137–152. doi: 10.1016/S0001-8686(98)00044-X.
28. Su X, Wang X, Ge Z, et al. KOH-activated biochar and chitosan composites for efficient adsorption of industrial dye pollutants. *Chemical Engineering Journal*. 2024; 486: 150387. doi: 10.1016/j.cej.2024.150387.
29. Gahrouei AE, Vakili S, Zandifar A, et al. From wastewater to clean water: Recent advances on the removal of metronidazole, ciprofloxacin, and sulfamethoxazole antibiotics from water through adsorption and advanced oxidation processes (AOPs). *Environmental Research*. 2024; 252: 119029. doi: 10.1016/j.envres.2024.119029.
30. John Y, David Jr VE, Mmerek D. A Comparative Study on Removal of Hazardous Anions from Water by Adsorption: A Review. *International Journal of Chemical Engineering*. 2018; 2018: 3975948. doi: 10.1155/2018/3975948.
31. Lawtae P, Tangsathikulchai C. The Use of High Surface Area Mesoporous-Activated Carbon from Longan Seed Biomass for Increasing Capacity and Kinetics of Methylene Blue Adsorption from Aqueous Solution. *Molecules*. 2021; 26(21): 6521. doi: 10.3390/molecules26216521.
32. Charmas B, Zięzio M, Jedynek K. Assessment of the Porous Structure and Surface Chemistry of Activated Biocarbons Used for Methylene Blue Adsorption. *Molecules*. 2023; 28(13): 4922. doi: 10.3390/molecules28134922
33. Amode JO, Santos JH, Md. Alam Z, et al. Adsorption of methylene blue from aqueous solution using untreated and treated (*Metroxylon* spp.) waste adsorbent: Equilibrium and kinetics studies. *International Journal of Industrial Chemistry*. 2016; 7: 333–345. doi: 10.1007/s40090-016-0085-9.
34. Sukmana H, Tombác E, Ballai G, et al. Comparative Study of Adsorption of Methylene Blue and Basic Red 9 Using Rice Husks of Different Origins. *Recycling*. 2023; 8(5): 74. doi: 10.3390/recycling805007.
35. Wei W, Yang L, Zhong WH, et al. Fast Removal of Methylene Blue from Aqueous Solution by Adsorption onto Poorly Crystalline Hydroxyapatite Nanoparticles. *Digest Journal of Nanomaterials and Biostructures*. 2015; 10(4): 1343–1363.
36. Plazinski W, Rudzinski W, Plazinska A. Theoretical models of sorption kinetics including a surface reaction mechanism: A review. *Advances in Colloid and Interface Science*. 2009; 152(1–2): 2–13. doi: 10.1016/j.cis.2009.07.009.
37. Tran HN. Applying Linear Forms of Pseudo-Second-Order Kinetic Model for Feasibly Identifying Errors in the Initial Periods of Time-Dependent Adsorption Datasets. *Water*. 2023; 15(6): 1231. doi: 10.3390/w15061231.
38. Silva LMS, Muñoz-Peña MJ, Domínguez-Vargas JR, et al. Kinetic and equilibrium adsorption parameters estimation based on a heterogeneous intraparticle diffusion model. *Surfaces and Interfaces*. 2021; 22: 100791. doi: 10.1016/j.surfin.2020.100791.
39. Wang Y, Srinivasakannan C, Wang H, et al. Preparation of novel biochar containing graphene from waste bamboo with high methylene blue adsorption capacity. *Diamond and Related Materials*. 2022; 125: 109034. doi: 10.1016/j.diamond.2022.109034.
40. Cantu Y, Remes A, Reyna A, et al. Thermodynamics, kinetics, and activation energy studies of the sorption of chromium (III) and chromium (VI) to a Mn₃O₄ nanomaterial. *Chemical Engineering Journal*. 2014; 254: 374–383. doi: 10.1016/j.cej.2014.05.110.
41. Ji B, Wang J, Song H, Chen W. Removal of methylene blue from aqueous solutions using biochar derived from a fallen leaf by slow pyrolysis: Behavior and mechanism. *Journal of Environmental Chemical Engineering*. 2019; 7(3): 103036. doi: 10.1016/j.jece.2019.103036.
42. Lyu H, Gao B, He F, et al. Experimental and modeling investigations of ball-milled biochar for the removal of aqueous methylene blue. *Chemical Engineering Journal*. 2018; 335: 110–119.
43. Huang W, Chen J, Zhang J. Adsorption characteristics of methylene blue by biochar prepared using sheep, rabbit and pig manure. *Environmental Science and Pollution Research*. 2018; 25: 29256–29266. doi: 10.1007/s11356-018-2906-1.

44. Wang J, Tan Y, Yang H, et al. On the adsorption characteristics and mechanism of methylene blue by ball mill modified biochar. *Scientific Reports*. 2023; 13: 21174. doi: 10.1038/s41598-023-48373-1.
45. Ge Q, Li P, Liu M, et al. Removal of methylene blue by porous biochar obtained by KOH activation from bamboo biochar. *Bioresources and Bioprocessing*. 2023; 10: 51. doi: 10.1186/s40643-023-00671-2.
46. Martis LJ, Parushuram N, Sangappa Y. Preparation, characterization, and methylene blue dye adsorption study of silk fibroin–graphene oxide nanocomposites. *Environ. Sci.: Adv.* 2022; 1: 285–296. doi: 10.1039/D1VA00047K.
47. El Messaoudi N, El Khomri M, El Mouden A, et al. Regeneration and reusability of non-conventional low-cost adsorbents to remove dyes from wastewaters in multiple consecutive adsorption–desorption cycles: A review. *Biomass Conversion and Biorefinery*. 2024; 14: 11739–11756. doi: 10.1007/s13399-022-03604-9.
48. Luo X, Du H, Zhang X, et al. Amine-functionalized magnetic biochars derived from invasive plants *Alternanthera philoxeroides* for enhanced efficient removal of Cr (VI): Performance, kinetics and mechanism studies. *Environmental Science and Pollution Research*. 2022; 29: 78092–78106. doi: 10.1007/s11356-022-20987-4.
49. Rasouli J, Zandifar A, Rasouli K, et al. High-efficiency ternary CeO₂/WO₃/AC photocatalyst supported by biomass waste-derived activated carbon for efficient doxycycline photodegradation: Optimization of synthesis conditions and operational parameters. *Materials Research Bulletin*. 2024; 178: 112874. doi: 10.1016/j.materresbull.2024.112874.
50. Yu H, Zhang Y, Wang L, et al. Experimental and DFT insights into the adsorption mechanism of methylene blue by alkali-modified corn straw biochar. *RSC Advances*. 2024; 14: 1854–1865. doi: 10.1039/D3RA05964B.